Available online at www.sciencedirect.com

ScienceDirect

www.elsevier.com/locate/jmbbm

Research paper

Extracellular bone matrix exhibits hardening elastoplasticity and more than double cortical strength: Evidence from homogeneous compression of non-tapered single micron-sized pillars welded to a rigid substrate

Krzysztof W. Luczynski[a], *Andreas Steiger-Thirsfeld*[b], *Johannes Bernardi*[b], *Josef Eberhardsteiner*[a], *Christian Hellmich*[a,*]

[a]*Institute for Mechanics of Materials and Structures, Vienna University of Technology (TU Wien), Karlsplatz 13/202, 1040 Vienna, Austria*

[b]*University Service Center for Transmission Electron Microscopy, Vienna University of Technology (TU Wien), Wiedner Hauptstrasse 8-10, 1040 Vienna, Austria*

ARTICLE INFO

Article history:
Received 17 October 2014
Received in revised form
13 February 2015
Accepted 1 March 2015
Available online 7 March 2015

Keywords:
Bone
Focused ion beam milling
Homogeneous strain state
Micropillars
Unloading
Elastoplasticity

ABSTRACT

We here report an improved experimental technique for the determination of Young's modulus and uniaxial strength of extracellular bone matrix at the single micrometer scale, giving direct access to the (homogeneous) deformation (or strain) states of the tested samples and to the corresponding mechanically recoverable energy, called potential or elastic energy. Therefore, a new protocol for Focused Ion Beam milling of prismatic non-tapered micropillars, and attaching them to a rigid substrate, was developed. Uniaxial strength turns out as at least twice that measured macroscopically, and respective ultimate stresses are preceded by hardening elastoplastic states, already at very low load levels. The unloading portion of quasi-static load–displacement curves revealed Young's modulus of 29 GPa in bovine extracellular bone matrix. This value is impressively confirmed by the corresponding prediction of a multiscale mechanics model for bone, which has been comprehensively validated at various other observation scales, across tissues from the entire vertebrate animal kingdom.

1. Introduction

Inelastic deformation of bone material is often associated with the formation and evolution of microcracks, exhibiting a characteristic size of some tens of micrometers (Schaffler et al., 1994, 1995; Wenzel et al., 1996; O'Brien et al., 2000; Chapurlat et al., 2007). These microcracks are already found in bone samples harvested from specific anatomical sites, as was evidenced for human adult ribs (Schaffler et al., 1994; O'Brien et al., 2000), human femur (Schaffler et al., 1995), human vertebral bone

*Corresponding author.
E-mail address: christian.hellmich@tuwien.ac.at (C. Hellmich).

http://dx.doi.org/10.1016/j.jmbbm.2015.03.001

(Wenzel et al., 1996), postmenopausal human transiliac bone (Chapurlat et al., 2007); and they grow under homogeneous loading of millimeter-sized bone samples in fatigue tests (Reilly and Currey, 1999; Akkus and Rimnac, 2001; O'Brien et al., 2003; Nicolella et al., 2011). The aforementioned microcracks are thought to interact with tens-of-micrometers-sized objects, such as lacunar pores (Reilly and Currey, 1999; Hamed and Jasiuk, 2013) or cement lines around osteons (Hamed and Jasiuk, 2013; Katsamenis et al., 2013; Nobakhti et al., 2014). It is theoretically well accepted that no cracks occur at the single nanometer scale (Gao et al., 2003), and this is in accordance with transmission electron micrographs of single bone mineral crystals (Ziv and Weiner, 1994; Kim et al., 1995, 1996; Zylberberg et al., 1998; Su et al., 2003). Comparatively, the situation at the single-micron scale is only vaguely investigated, and therefore, rather poorly understood. The reason for this is twofold: (i) a purely theoretical investigation as in the case of hydroxyapatite is a tremendous challenge due to the complex micro-heterogeneous nature of the material at the single microns-scale; (ii) experimental approaches undertaken at that scale, such as the many nanoindentation campaigns during the last two decades (Ko et al., 1995; Roy et al., 1996; Rho et al., 1997, 1999a,b; Hoffler et al., 1997; Turner et al., 1999; Rho and Pharr, 1999; Zysset et al., 1999; Fan et al., 2002; Hengsberger et al., 2002; Ebenstein and Pruitt, 2006), exhibit strong stress and strain gradients. Namely, the latter impede direct determination of continuum mechanical properties like stiffness or strength, which are, by definition (Salencon, 2001; Zaoui, 2002), related to homogeneous stress or strain states imposed onto a representative volume element of solid matter. In order to overcome this problematic situation, an increasing number of researchers have more recently been investing into the Focused Ion Beam (FIB) milling technique, allowing them to carve out micropillars from a surrounding substrate. Some of them carved out horizontally oriented beams, which were then subjected to bending deformations (Jimenez-Palomar et al., 2012; Chan et al., 2009). Retrieving elastic properties from such, strictly speaking, structural tests inducing inhomogeneous stress and strain states requires the use of beam theories and respective inherent assumptions. In order to do without the latter, many researchers have produced vertically oriented pillars, and have compressed them by flat punches, so as to induce quasi-homogeneous stress states within the aforementioned micropillars (Barnoush et al., 2010; Battaile et al., 2012; Dietiker et al., 2011; Frick et al., 2007, 2008a,b; Kheradmand et al., 2013; Kirchlechner et al., 2011; Monnet and Pouchon, 2013; Nagoshi et al., 2013, 2014; Ng et al., 2011; Ng and Ngan, 2008; Raghavan et al., 2012; Schneider et al., 2009, 2011, 2013; Schwiedrzik et al., 2014; Stewart et al., 2012; Yang et al., 2009; Zhang et al., 2010). However, even if the problems of pillar tapering (a phenomenon which restricts stress and strain homogeneity to the pillar cross sections, while the stress magnitudes within the pillar decrease with increasing distance from the flat punch) are solved, see e.g. Kinashi et al. (2014), Kirchlechner et al. (2011), Mutoh et al. (2013), and Nagoshi et al. (2013, 2014) for the production of non-tapered pillars, then these tests still do not allow for direct determination of stiffness or strength values, since the machine-measured displacements of the quasi-rigid punch do not only relate to the deformations of the pillar itself, but also to those of the elastic half space below. The current contribution aims at meeting exactly this last challenge on the way to a truly continuum mechanical test at the single-micron scale, and to apply a correspondingly developed experimental protocol to bone. In more detail, the challenge lies in the production of non-tapered micropillars, and in detaching them from the original (deformable) substrate, so as to plant them onto a rigid substrate. To the very best knowledge of the authors, this has never been reported before – and the remainder of the paper is devoted to a concise description of the protocol, and a first batch of results obtained on miniature samples harvested from bovine cortical bone.

2. Materials and methods

2.1. *Sample production*

In order to arrive at the targeted non-tapered micropillars welded to a rigid substrate, the following sequence of processing steps was realized: first of all, a portion of an 18 month-old bovine femur was obtained from a local butcher [see Figs. 1(a) and 3(a)]. A hand saw was used to cut the aforementioned portion along the long bone axis, yielding smaller parts as seen in Figs. 1(b) and 3(b). Then, ten slices of approximately 1 mm thickness were cut, by means of a diamond saw (Isomet, Buehler, USA), from the aforementioned smaller parts. Thereby, the cutting direction was orthogonal to the long bone axis [see Figs. 1(b) and 3(b)]. Afterwards, the aforementioned slices [see Fig. 3(c)] were cut into again smaller pieces with dimensions of approximately $7 \times 2 \times 1$ mm [see Fig. 3(d)], and the latter were then kept frozen at $-20\,^{\circ}C$ (Fölsch et al., 2011; Nazarian et al., 2009; Linde and Sørensen, 1993), in order to preserve their mechanical properties throughout the time lag between slice production and investigation of their single micron-scale elasticity and strength. For the latter purpose, the small pieces were, one after the other, unthawed and processed separately, in order to reduce the time of exposure to potentially harming environmental factors. FIB-milling is done under vacuum, and in order to prevent (i) possible vacuum pump-induced formation of drying cracks in the investigated specimens (Jimenez-Palomar et al., 2012), (ii) their negative charging under the SEMs electron beam (resulting in beam deflection, which may cause loss of resolution or astigmatism) (Bourne, 1972), as well as (iii) FIB-induced positive charging (which may lead to "surface melting" caused by incident Ga^{+} ions) (Nalla et al., 2005; Stokes et al., 2006; Drobne et al., 2007), each of the platy pieces described before, was coated by a 17 nm thick gold-palladium sheet (SC502-314B target, Quorum Technologies Ltd, East Sussex, United Kingdom) using the Q150T S High Resolution Sputter Coater (Quorum Technologies Ltd, East Sussex, United Kingdom).

The next major task was to mill, out of the aforementioned pieces, tiny micro-pillars in the Quanta 200 3D DualBeam (FEI, Hillsboro, Oregon, USA). The latter system is equipped with a vacuum chamber, an adjustable sample stage, a Focused Ion Beam (FIB), a Scanning Electron Microscope (SEM), and an in-built nano-manipulator (Kleindiek Nanotechnik GmbH, Reutlingen, Germany). The first Quanta-related processing step concerns its pin-mount sample holder to which both one of the tiny bone pieces and a silicon wafer (which would serve a s future "rigid" substrate for the micropillar samples) were glued, by means of a conductive silver adhesive (Plano GmbH,

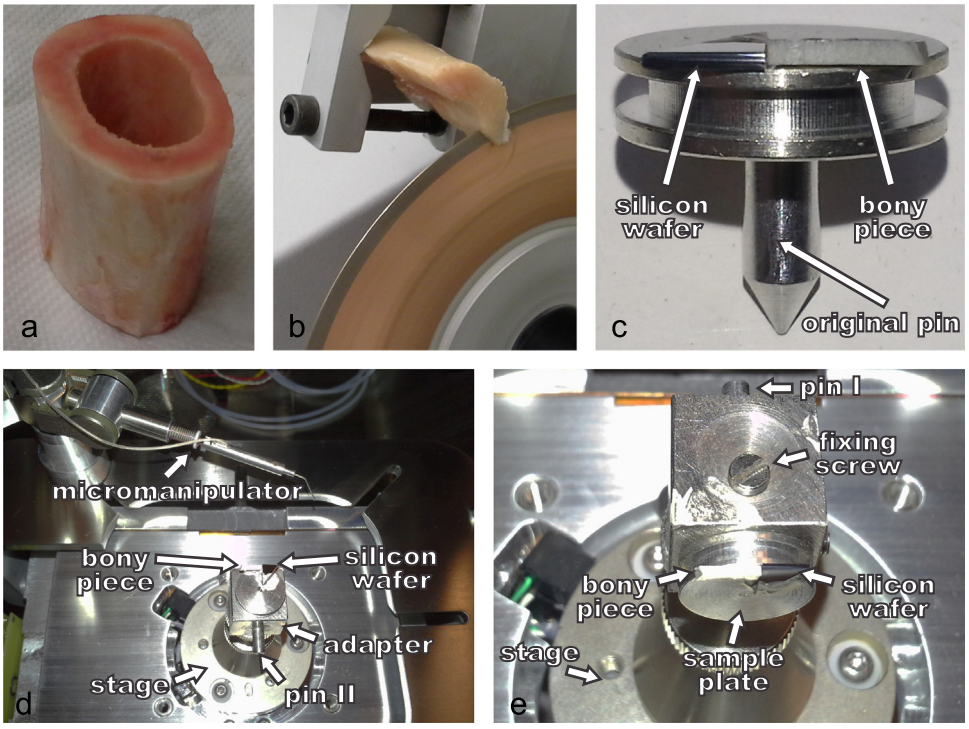

Fig. 1 – Sample preparation steps: (a) a portion of bovine femur as obtained from a local butcher; (b) cutting of an approximately 1 mm thick slice; (c) bony piece and silicon wafer glued to a pin-mount sample holder; (d) pin-mount sample holder mounted on the stage of FIB-milling device via the cubical adapter, which is attached to the stage by means of "pin I" [see Fig. 2(a)]; this enables FIB-milling parallel to the long bone axis, i.e. cutting the side walls of a pillar; (e) bony piece rotated by 90° as compared to (d), through attachment of the adapter to the stage by means of "pin II" [see Fig. 2(b)]; this enables FIB-milling perpendicular to the long bone axis, e.g. cutting off the sample.

Wetzlar, Germany), see Figs. 1(c) and 2. This sample plate needs to be able to be located within the Quanta instrument both orthogonal *and* parallel to the ion beam, in order to allow for cutting both the side walls and the bottom surface of the desired micropillar specimens. Since both of the aforementioned configurations cannot be realized by means of tilting the Quanta stage (which allows orthogonality and obliquity, but not parallelity of the sample plate and the ion beam), a cubical adapter was designed, see Fig. 2. It carries the pin-mount sample holder, through a hole with screw fixation, on one of its faces, and can then be fixed, by means of one out of two orthogonal pins, to the Quanta 200 stage. One of these two pins is positioned on the cube's face which is opposite of that hosting the sample plate, and the other one on a face orthogonal to the two aforementioned faces; these two pins are denoted as "pin I" and "pin II" in Fig. 2. The respective plate-adapter compound was then attached to the stage, first by means of "pin I", in order to enable milling in axial bone direction, defining the long axis of the pillars to be produced [see Figs. 1(d) and 2(a)].

Then, the top surface of the bony piece was carefully scanned, so as to identify a plain area, which did not show any traces of lacunar or canalicular pores cut during the sawing process. Naturally, this scanning procedure alone does not rule out the sheer possibility of the presence of canaliculi or lacunae inside the samples to be produced. In the end, the presence of such pores, which are not negligible in size when compared to the finally FIB-produced micropillars, would express themselves in very low stiffness and strength values of the latter, when compared to non-porous pillars. Respective details are given in the Results section. Particularly, three quadratic areas with roughly 3 μm side length were chosen in the immediate proximity of the edge shared by the top surface and the diamond saw-cut (1 mm high) "front wall" of the bony piece [see Fig. 3(d)]. These areas were coated, by means of a 0.3 nA current, with platinum (Pt), so as to protect the bony material underneath, while FIB-cleaning the aforementioned "front wall" by means of a 3 nA gallium (Ga^+) beam oriented in the longitudinal bone direction [see Fig. 3(e) for a schematic drawing]. Afterwards, the material surrounding the three other sides of the platinum-coated areas was removed by means of FIB-milling with a 3 nA gallium ion beam [see Fig. 3(f)]: this resulted in the production of three prismatic pillars with temper angles of about 2° (getting thicker towards their bottom), and with a cross-sectional area which was slightly larger than finally desired. In order to then reach the final specimen shape, the side walls of the pillars under fabrication were set at an angle of 4° with respect to the FIB column (therefore, the stage was inclined by 2°), and a 1 nA Ga^+ current was employed for correcting the initial temper angle. This resulted in regular quadratic prisms with cross-sectional side dimensions of roughly 1.3 μm, see Fig. 4(a,b).

In order to cut off the pillars from the remaining bone mass, the vacuum chamber was shortly opened, the previously mentioned self-designed adapter (with the pin-mount sample plate attached to it) was first removed, and then re-mounted

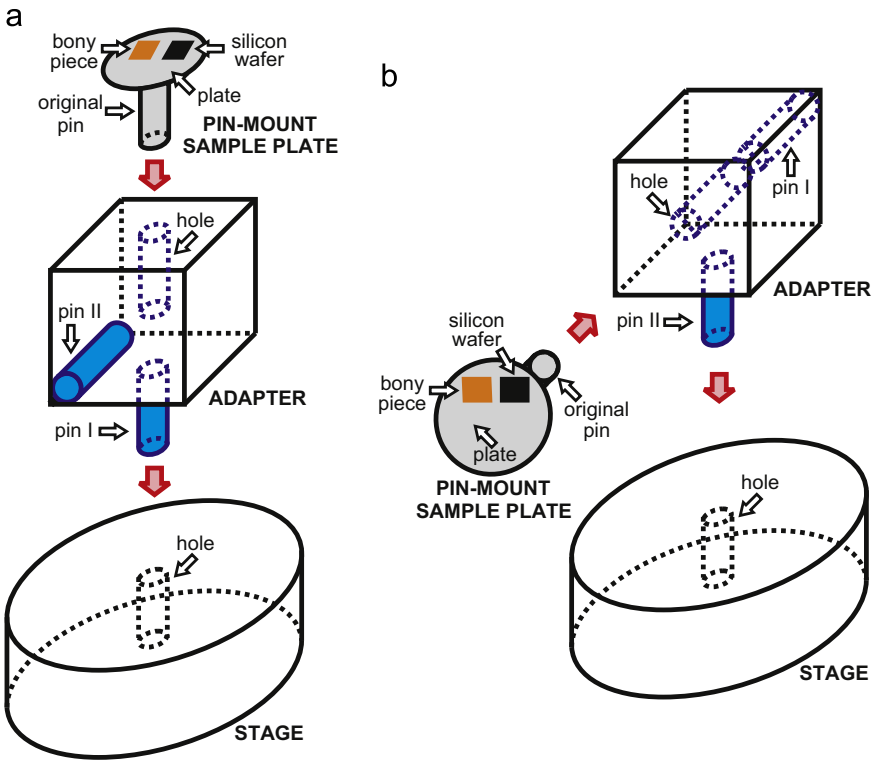

Fig. 2 – Schematic illustration of how the bony piece is mounted to the stage of the Quanta 200 3D DualBeam system: (a) for FIB-milling of the side walls of micropillars and (b) for cutting off the completely carved micropillars from the remaining material.

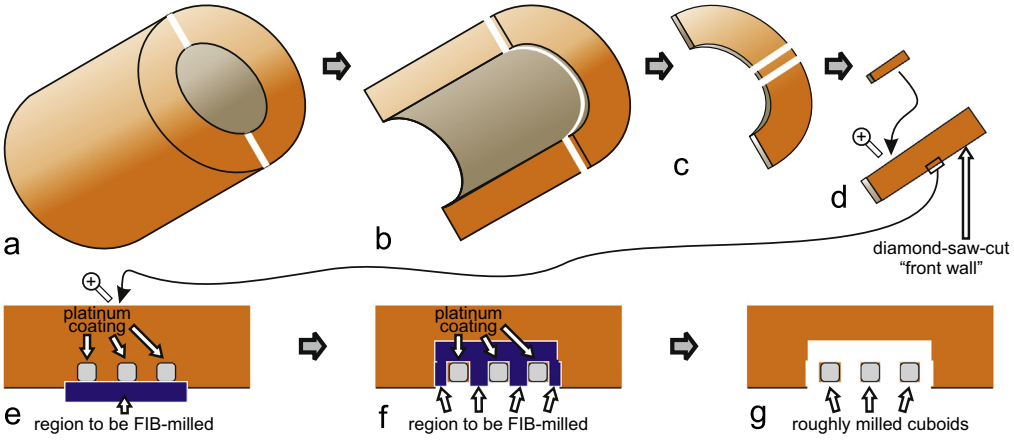

Fig. 3 – Schematic drawing of sample preparation steps, from cutting of the macroscopic bone until rough FIB-milling of cuboids: (a) a portion of bovine femur as obtained from a local butcher; (b) a hand-saw-cut part of the bone, which is small enough for subsequent diamond saw cutting; (c) 1 mm thick slice, diamond-saw-cut orthogonal to the long bone axis; (d) a diamond -saw-cut platy piece, prepared for FIB milling; (e) FIB-cleaning of the diamond-saw-cut "front wall"; (f) rough FIB-milling of the "side walls" and of the "back wall"; (g) roughly milled prisms with a cross-sectional surface area slightly larger than desired, and with a temper angle of approximately 2°.

onto the sample stage, but this time through "pin II" [see Figs. 1 (e) and 2(b)]. After localizing the previously produced micropillars using the built-in SEM, the manipulator needle was attached to the top of the first cuboid by means of ion-beam-induced tungsten (W) deposition (IBID). Then the bottom of the pillar was cut off through a 1 nA Ga^+ current [see Fig. 4(c)]. The needle together with the cut-off cuboid was then moved to the silicon wafer positioned next to the bony slice, and the cuboid was very carefully placed onto this wafer [see Fig. 4(d)] and attached to it, using again an ion-beam-induced tungsten deposition.

Subsequently, the 1 nA current was employed to separate the top part of a pillar (still attached to the needle) from its bottom, in order to produce a micropillar characterized by an aspect ratio (defined as height over width) of roughly four. In case the remaining top part of the cuboid was high enough,

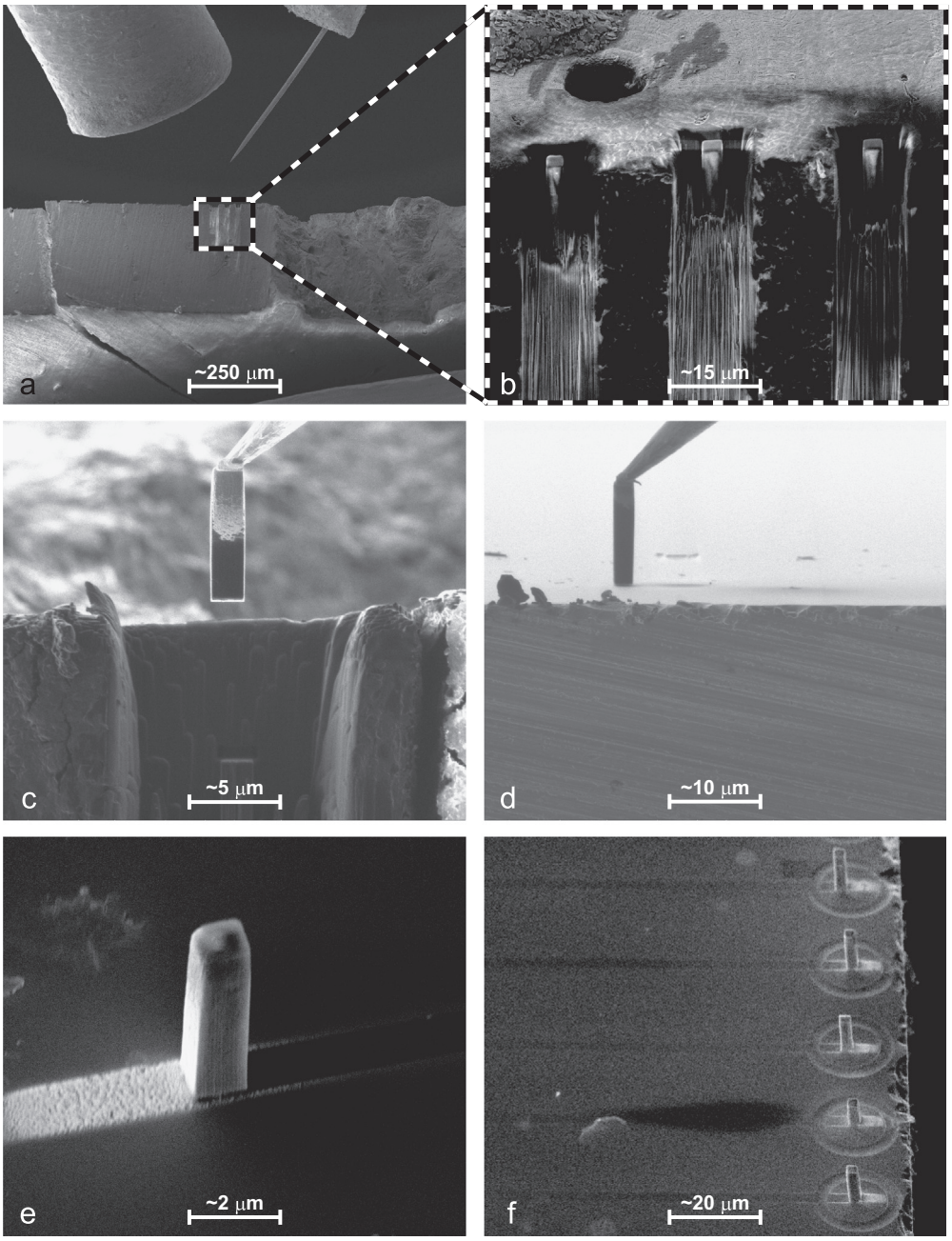

Fig. 4 – FIB-milling in Quanta 200 instrument: (a) SEM-image of the bony piece (at the bottom), of the tungsten source (left upper corner), and of the micromanipulator needle (right upper corner); (b) SEM-image of quadratic prisms with the side walls already separated from the surrounding material; (c) FIB-image of a lifted micropillar attached to the micromanipulator needle; (d) FIB-image of a pillar placed on the silicon substrate and still attached to the micromanipulator needle; (e) SEM-image of a completed micropillar placed on the silicon substrate; (f) SEM-image of five micropillars, as later tested in the nanoindenter; FIB-milled shallow circles around each pillar help us to localize the samples with the low resolution light microscope built into the used nanoindenter.

another pillar was produced applying the same procedure (i.e. the micropillar was again carefully placed onto the silicon wafer, attached to it and the surplus part together with the needle was cut off). Finally, the very top of each micropillar was "cleaned" by means of Ga^+ current of 0.1 nA. The whole operation of cutting-off the prismatic specimen and placing it on the wafer was repeated for the remaining cuboids, and depending on the cuboids' heights and on the overall success of the manually challenging procedure, each platy bone piece allowed for the production of a set of two to five cortical bone pillars with square cross-sections, welded to a silicon wafer [see Fig. 4(e) for a single "zoomed-in" sample, and Fig. 4(f) for a set of five samples, respectively]. As the next step, a shallow circle was milled around each pillar, in order to enable localization of the samples by means of the low resolution light microscope built into the subsequently used

nanoindenter (TI 900 Triboindenter, Hysitron, Minnesota, USA). Afterwards, all samples were inspected for any visible pores or production deficiencies, and their height and cross-sectional edge length dimensions were measured by means of SEM-imaging. Finally, all pillars having passed the visual surface inspection were then promptly tested in a nanoindenter, as described next. Concerning processing time, the whole procedure, from removing a pre-cut bony piece from the freezer until testing in the nanoindenter, did not last any longer than 30 h. Such "drying conditions" are obviously much less severe than exposure to high vacuum, and even the latter has been shown to only extract the free water, but not the bound water from (macroscopic) bone samples (Jimenez-Palomar et al., 2012). However, micropillars without canalicular or lacunar pore remnants contain only bound water, so that no remarkable effect of the environmental conditions on the tested mechanical properties is expected: they refer to "wet extracellular (ultrastructural) bone matrix". Actually, Jimenez-Palomar et al. (2012) have even explicitly shown that mechanical properties determined from micropillar tests are indeed independent of the environmental testing conditions.

2.2. *Mechanical testing*

Each micro-pillar was compressed by a flat-punch (flat-ended cone with 10 μm flat-end-radius and 90° cone angle, HYS-TI-0227, Hysitron, Minnesota, USA) under displacement-control. More specifically, a trapezoidal load function was employed: first, a quasi-static sample-specific displacement rate corresponding to a strain rate of $0.005\,s^{-1}$, which is typical for biomaterials testing (Brynk et al., 2011; Luczynski et al., 2013), was prescribed, up to a sample-specific maximum compressive displacement corresponding to -0.05 nominal strain. Then, the displacement was kept constant for 10 s; thereafter, the specimen was unloaded at the same strain rate as employed before. Raw data obtained from the nanoindenter software in terms of prescribed displacements, and correspondingly recorded forces, were converted into axial stress and strain components, based on the specimens' heights and cross-sectional edge dimensions. Young's modulus of the material making up the micropillars was derived from the linear portion of the unloading branch of the quasi-static tests following an earlier published protocol (Luczynski et al., 2013). In more detail, the unloading path was split into intervals amounting to 1% of the maximum strain level achieved before (corresponding to approximately 2 nm), and increasingly long portions of the unloading path (in terms of multiples of the aforementioned intervals) were linearly fitted, resulting in a portion-specific slope and coefficient of determination (R^2). The slope corresponding to the unloading portion with the highest R^2 (the "most linear" unloading path) was then considered as Young's modulus of the investigated sample.

3. Results

After FIB-milling, 13 samples passed the SEM-supported visual inspection concerning undesired pore remnants or production deficiencies. These 13 samples were mechanically tested, which showed that four samples exhibited an almost vanishing strength, which probably resulted from undetected processing damage or internal, and therefore invisible, lacunar or canalicular pores. Thus, the mechanical tests on the remaining $n=9$ samples were further analyzed. The corresponding force-to-stress and displacement-to-strain conversions were based on the measured length dimensions of the samples, as given in Table 1. They are characterized by average values and standard deviations of $h=4.97\pm0.28$ μm and $a=1.27\pm0.14$ μm, respectively.

The resulting stress–strain characteristics, depicted in Fig. 5, clearly show the elastoplastic nature of the tested samples, since the initial slope of the loading portion is always smaller than the unloading portion's slope recorded at the maximum applied strain, and indicated in Fig. 5 as a thick solid line. The linear fits of all unloading portions were always characterized by a coefficient of determination larger than 99%, $R^2>0.99$; and they delivered values of Young's moduli characterized by an average and a standard deviation of $E=29.09\pm2.39$ GPa. Six samples "failed" under the applied strain level, i.e. their stress–strain curve did not show a monotonous increase, but maximum stress values, i.e. ultimate strengths, amounting to $\sigma_{ult}=505.1\pm87.5$ MPa. The corresponding ultimate strain amounted to $\varepsilon_{ult}=0.0374\pm0.0077$. Three out of the nine aforementioned samples withstood the applied compressive stress, i.e. during loading the stress increased monotonously with the applied strain. Thereby, the attained maximum stress levels amounted to 646.4 ± 24.3 MPa – with actual strength values of these samples being obviously higher than these values – and the respective ultimate strains exceeding the magnitude of 0.05.

Table 1 – Length dimensions of prismatic micropillars; sample labels correspond to the single stress–stain characteristics in Fig. 5.

Sample name	Height h(μm)	Side length a(μm)	Aspect ratio (–)
a	4.46	1.11	4.02
b	4.67	1.18	3.96
c	5.11	1.17	4.37
d	4.78	1.28	3.73
e	5.05	1.20	4.21
f	5.32	1.20	4.43
g	5.07	1.38	3.67
h	5.26	1.57	3.35
i	5.03	1.36	3.70

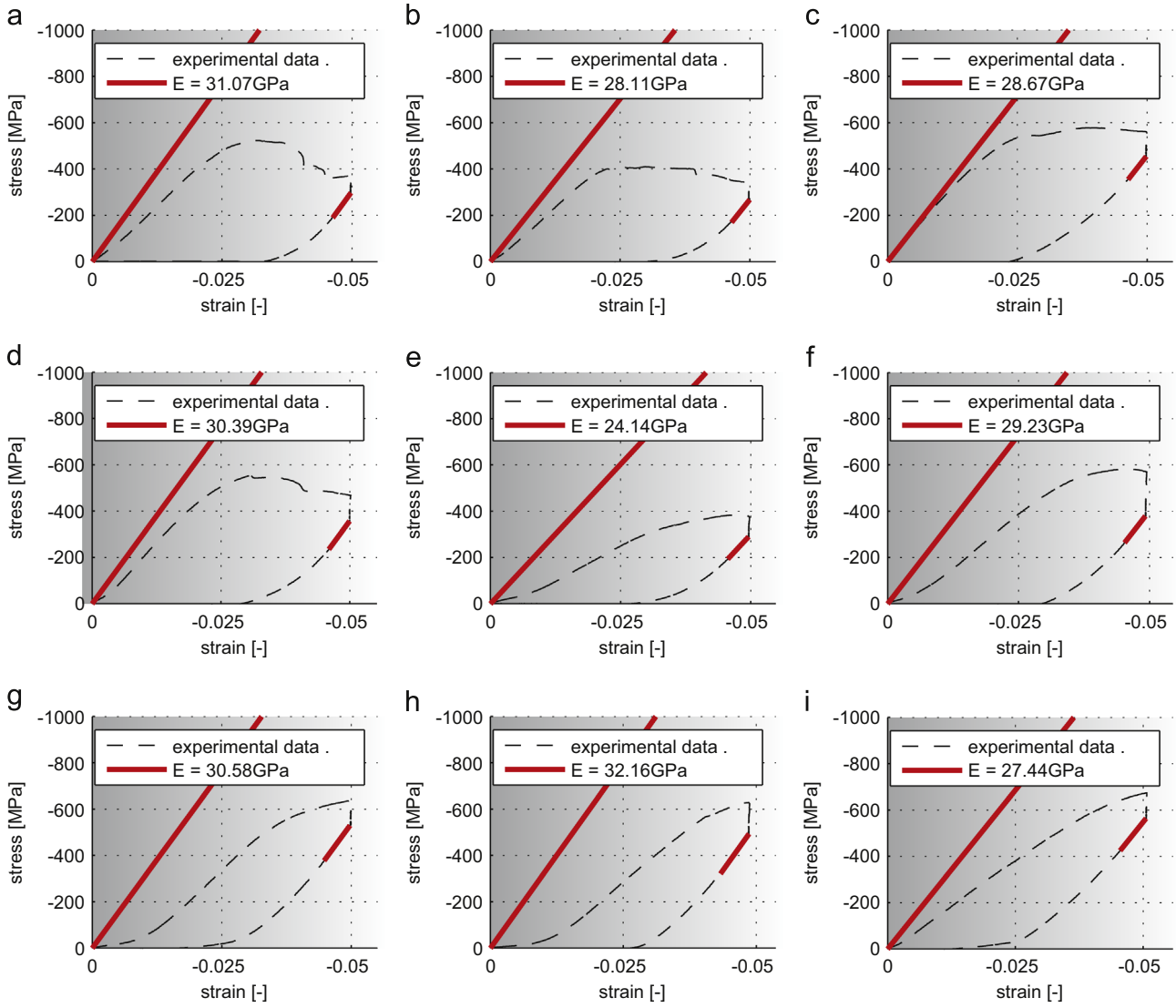

Fig. 5 – Stress–strain characteristics derived from flat punch micropillar tests; for samples failing under applied load (a)–(f), and for samples having withstood the test (g)–(i); red solid lines indicate the slope related to Young's modulus, as derived from the unloading branch; shifting this slope indication to the origin evidences inelastic material behavior during the loading regime; letters from (a) to (i) indicate sample names as used in Table 1. (For interpretation of the references to color in this figure caption, the reader is referred to the web version of this paper.)

4. Discussion

To our best knowledge, we presented here the very first quasi-static mechanical tests where homogeneous stress and strain states were applied to single micron-sized specimens made of extracellular bone matrix. Hence, they hold the promise to extend our fundamental understanding of the mechanical behavior of bone at the single micron observation scale and below. Thereby, our primary focus was on the determination of elastic properties, and in this context, we take a strictly thermodynamic viewpoint, considering that the mechanics of materials was successfully reconciled with the fundamental laws of thermodynamics about half a century ago, as is described in great detail in various standard textbooks, such as Mandel (1966), Salencon (2001), and Lurie and Belyaev (2005). Accordingly, the elastic behavior is related to the potential or free energy stored upon deformation in the considered body. Upon unlaoding, this energy is transformed into efficient mechanical work done by the material sample on its surroundings. Hence, as long as work is put into the material system (e.g. during the loading phase in a uniaxial test), the internal energy of this system is increased, but it is not clear which portion of this energy may still be recovered in terms of efficient mechanical work, and which portion is "lost" into heat (through dissipation). Hence, only the unloading portion gives direct access to the recoverable mechanical work, and consequently, to the elasticity of the material. If a material behaves purely elastically throughout a uniaxial test comprising loading and unloading regimes, then the loading and unlaoding branches in the stress–strain diagram fully coincide – this is not the case in our present study. If a

material behaves elastically up to a certain load level, called elastic limit, and shows dissipative (typically plastic) behavior afterwards, then the loading and unloading branches in the stress–strain diagram are still parallel – also this is not the case in our present study, where there is a remarkable difference between the loading and the unloading portions of the recorded force-to-displacement diagrams. Right from the beginning of the loading phase, more work is put into the system than would ever be recovered upon unloading – hence, the entire loading branch is of elastoplastic nature; more precisely, of hardening elastoplastic nature, since the stresses increase in magnitude upon increased deformation of the tested sample. The work recovered during unloading, on the other hand, gives access to the elastic energy which has been stored within the sample during the loading phase, and hence to its modulus of elasticity (in a strict thermodynamic sense). In this context, it is probably useful to mention a terminological issue arising with simulations in the field of bone biomechanics: unloading protocols, as used for more than two decades in the course of nanoindentation studies (Oliver and Pharr, 1992; Rho et al., 1997), deliver truly elastic properties. On the other hand, moduli derived from the loading portion of a stress–strain curve actually also contain information on inelastic, most probably plastic, deformation events. Consequently, if such moduli are used in formally "elastic" linear Finite Element analyses, as e.g. reported by Bevill and Keaveny (2009), then they represent, from a strictly physical standpoint, the material behavior known as "linear elasto-plastic hardening" (Coussy, 2010). Still, the discussion on deriving elastic moduli from the unloading branches of our uniaxial tests might well be extended by another intriguing subtlety, related to the question on whether the rather ideally plastic, or even slightly softening regimes in the stress–strain diagram, i.e. those portions where zero stress increments or slightly negative stress increments are related to strain increments further increasing the overall deformation, might have an detrimental effect on the elastic properties – this phenomenon is normally called damage in a mechanics of materials context (Kachanov, 1986), and it is explained as the effect of crack propagation within the tested material sample, as was also shown in the framework of micromechanics theory (Pichler et al., 2007). Such damage phenomena would be reflected by elastic moduli which decrease with increasing maximum load level which would have been attained in the uniaxial tests, see e.g. Hansen and Schreyer (1994) for an in-depth theoretical formulation of how the free (elastic) energy may depend on the degree of damage. However, such a systematic correlation between maximum load level and unloading modulus cannot be inferred from the curves depicted in Fig. 5. This proposes that no major cracking events occur during loading, and that the elastic moduli derived from the unloading portion of the stress–strain curves refer to a virtually undamaged material. This is fully consistent with reports on bone microcracking, all of these showing cracks larger than single microns (Schaffler et al., 1994, 1995; Wenzel et al., 1996; O'Brien et al., 2000; Chapurlat et al., 2007); and which is also confirmed with earlier propositions to consider frictional or elastoplastic events as the origin of bone strength (Tai et al., 2006; Fritsch et al., 2009b; Ritchie, 2011). The absence of "damage" (as synonym of crack formation) was also implied from earlier tests made on tapered bone micropillars un-detached from the underlying (and also elastoplastic) half-space (Schwiedrzik et al., 2014). Moreover, it is notable that our measured strength values of extracellular bone matrix are by a factor of about 2.5 higher than those measured macroscopically (Burstein et al., 1972; Reilly et al., 1974; Cezayirlioglu et al., 1985). However, these quite surprisingly high values can still be seen just as lower bounds for the actual strength of the material, since some samples reached higher stress levels without even failing.

Yet, the strongest novelty of our results may be the possibility to directly determine Young's modulus of the extracellular matrix, amounting to $E=29.09\pm2.39$ GPa in bovine tibial bone. Since we are not aware of similar tests, we cannot directly compare this number to one obtained in earlier experiments. Nevertheless, we may check the relevance of this number by comparing it to the numerical prediction of a suite of mathematical models (Hellmich and Ulm, 2003; Morin and Hellmich, 2013; Morin et al., 2013; Morin and Hellmich, 2014), which consistently integrate a wealth of biochemical, biophysical, and biomechanical data gathered in different laboratories on different bones of differently aged organisms, and different anatomical locations. The premise of these microstructural and micromechanical theories and corresponding mathematical models is that the mechanical properties of bone at different length scales can be predicted from the tissue-independent (universal) mechanical properties of the elementary building blocks of bone (hydroxapatite, collagen type I, gel-type water with non-collagenous organics), and their "universal" mechanical interaction patterns, while only their dosages are tissue-, age-, and anatomical location-dependent. But even these dosages follow yet another "universal" rules, affecting the collagen-to-mineral rations actually realized in mineralized tissues (Vuong and Hellmich, 2011), the mineral concentration in the extra-collagenous space (Hellmich and Ulm, 2003), or the fluid-to-solid phase transformation during mineralization (Morin and Hellmich, 2013; Morin et al., 2013). All these "universal" characteristics are in line with very many experimental results, comprising demineralization/ashing/de-collagenozation/drying test (Hammett, 1925; Chick et al., 1926; Burns, 1929; Gong et al., 1964; Biltz and Pellegrino, 1969; Lees, 1987, 2003; Lees et al., 1995), X-ray and neutron diffraction tests (Bonar et al., 1985; Lees et al., 1984) as well as ultrasonic and mechanical tests (Currey, 1959; Burstein et al., 1972; Reilly et al., 1974; Burstein et al., 1976; Lees et al., 1979, 1983, 1994; Lees, 1982; Cezayirlioglu et al., 1985; McCarthy et al., 1990); and the developed micromechanical theories hold for properties such as elasticity (Hellmich et al., 2004a,b; Fritsch and Hellmich, 2007); poro-elasticity (Hellmich and Ulm, 2005a,b; Morin and Hellmich, 2014); strength (Fritsch et al., 2009a) and creep (Eberhardsteiner et al., 2014) properties. Altogether, they imply that it is solely the extracellular mass density which by far governs the extracellular stiffness. In this context, we here adopt a mass density amounting to 2.04 ± 0.04 g/cm^3 (mean value$\pm$standard deviation), which was obtained from weighing of 22 samples tested by Lees et al. (1979). It may be surprising that this value is high as compared to BMD values for bovine cortical bone: the latter are normally determined from X-ray absorptiometry (Sasso et al., 2008), and they typically amount to 1.4 g/cm^3. However, the values of 2.0 g/cm^3 and 1.4 g/cm^3 actually fit

together very well, since BMD stands for "Bone Mineral Density", i.e. the mass of mineral per entire volume of bone matrix, a quantity also termed "apparent mass density of mineral". In fact, the demineralization tests of Lees et al. (1979) on exactly the aforementioned samples with 2.04 g/cm^3 mass density provide yet another access to this apparent mass density of the mineral, delivering again a value around 1.4 g/cm^3, for details on experimental protocols and corresponding evaluation schemes, see e.g. Vuong and Hellmich (2011). Inserting the aforementioned tissue mass density values of Lees et al. (1979), which agree very well with X-ray absorptiometry data revealing apparent mineral densities in bovine cortical bone, into the micromechanical formulation of Morin and Hellmich (2014) delivers Young's modulus of $E_{model} = 30.0 \pm 2.9$ GPa, which impressively confirms the relevance of our results obtained from unloading non-tapered micropillars. Namely, a one-way ANOVA performed on these 22 values stemming from the model and 9 values stemming from the conducted micro-pillar unloading tests indicates clearly ($p > 0.39$) that all these 31 values stem from the same statistical population. Conclusively, our unloading experiments performed on micro-pillars fully confirm the elastic properties of extracellular bone, as expected from a comprehensive micromechanical theory integrating biochemical, biomechanical, and biophysical information collected over one century at various laboratories.

Acknowledgments

Financial support within the project MICROBONE (Grant number 257023), granted by the ERC is gratefully acknowledged. Moreover, the authors are grateful for the involvement of the Laboratory Manager Enrico Dall'Ara during development of the test protocol.

REFERENCES

Akkus, O., Rimnac, C.M., 2001. Cortical bone tissue resists fatigue fracture by deceleration and arrest of microcrack growth. J. Biomech. 34 (6), 757–764.

Barnoush, A., Dake, J., Kheradmand, N., Vehoff, H., 2010. Examination of hydrogen embrittlement in FeAl by means of in situ electrochemical micropillar compression and nanoindentation techniques. Intermetallics 18 (July (7)), 1385–1389, http://dx.doi.org/10.1016/j.intermet.2010.01.001.

Battaile, C.C., Boyce, B.L., Weinberger, C.R., Prasad, S.V., Michael, J. R., Clark, B.G., 2012. The hardness and strength of metal tribofilms: an apparent contradiction between nanoindentation and pillar compression. Acta Mater. 60 (February (4)), 1712–1720, http://dx.doi.org/10.1016/j.actamat.2011.11.059.

Bevill, G., Keaveny, T., 2009. Trabecular bone strength predictions using finite element analysis of micro-scale images at limited spatial resolution. Bone 44 (4), 579–584.

Biltz, R., Pellegrino, E., 1969. The chemical anatomy of bone. J. Bone Jt. Surg. 51-A (3), 456–466.

Bonar, L.C., Lees, S., Mook, H., 1985. Neutron diffraction studies of collagen in fully mineralized bone. J. Mol. Biol. 181 (2), 265–270.

Bourne, G.H., 1972. The Biochemistry and Physiology of Bone. Volume I: Structure. Academic Press, New York, NY, USA.

Brynk, T., Hellmich, C., Fritsch, A., Zysset, P., Eberhardsteiner, J., 2011. Experimental poromechanics of trabecular bone strength: role of Terzaghi's effective stress and of tissue level stress fluctuations. J. Biomech. 44 (February (3)), 501–508, http://dx.doi.org/10.1016/j.jbiomech.2010.09.016.

Burns, C., 1929. The effect of the continued ingestion of mineral acid on growth of body and bone and on the composition of bone and of the soft tissues. Biochem. J. 23 (5), 860–867.

Burstein, A., Reilly, D., Martens, M., 1976. Aging of bone tissue: mechanical properties. J. Bone Jt. Surg. 58 (1), 82–86.

Burstein, A.H., Currey, J.D., Frankel, V.H., Reilly, D.T., 1972. The ultimate properties of bone tissue: the effects of yielding. J. Biomech. 5 (1), 35–44.

Cezayirlioglu, H., Bahniuk, E., Davy, D., Heiple, K., 1985. Anisotropic yield behavior of bone under combined axial force and torque. J. Biomech. 18 (1), 61–69.

Chan, Y., Ngan, A., King, N., 2009. Use of focused ion beam milling for investigating the mechanical properties of biological tissues: a study of human primary molars. J. Mech. Behav. Biomed. Mater. 2 (4), 375–383 〈http://www.sciencedirect.com/science/article/pii/S1751616109000174〉.

Chapurlat, R.D., Arlot, M., Burt-Pichat, B., Chavassieux, P., Roux, J.P., Portero-Muzy, N., Delmas, P.D., 2007. Microcrack frequency and bone remodeling in postmenopausal osteoporotic women on long-term bisphosphonates: a bone biopsy study. J. Bone Miner. Res. 22 (10), 1502–1509, http://dx.doi.org/10.1359/jbmr.070609.

Chick, H., Korenchevsky, V., Roscoe, M., 1926. The difference in chemical composition of the skeletons of young rats fed (1) on diets deprived of fat-soluble vitamins and (2) on a low phosphorus rachitic diet, compared with those of normally nourished animals of the same age. Biochem. J. 20 (3), 622–631.

Coussy, O., 2010. Mechanics and Physics of Porous Solids. John Wiley, Chichester, UK.

Currey, J., 1959. Differences in the tensile strength of bone of different histological types. J. Anat. 93 (1), 87–95.

Dietiker, M., Buzzi, S., Pigozzi, G., Lffler, J., Spolenak, R., 2011. Deformation behavior of gold nano-pillars prepared by nanoimprinting and focused ion-beam milling. Acta Mater. 59 (March (5)), 2180–2192, http://dx.doi.org/10.1016/j.actamat.2010.12.019.

Drobne, D., Milani, M., Leer, V., Tatti, F., 2007. Surface damage induced by FIB milling and imaging of biological samples is controllable. Microsc. Res. Tech. 70 (10), 895–903, http://dx.doi.org/10.1002/jemt.20494.

Ebenstein, D.M., Pruitt, L.A., 2006. Nanoindentation of biological materials. Nano Today 1 (3), 26–33.

Eberhardsteiner, L., Hellmich, C., Scheiner, S., 2014. Layered water in crystal interfaces as source for bone viscoelasticity: arguments from a multiscale approach. Comput. Methods Biomech. Biomed. Eng. 17 (1), 48–63, http://dx.doi.org/10.1080/10255842.2012.670227 PMID: 22563708.

Fan, Z., Swadener, J., Rho, J., Roy, M., Pharr, G., 2002. Anisotropic properties of human tibial cortical bone as measured by nanoindentation. J. Orthop. Res. 20 (4), 806–810.

Fölsch, C., Mittelmeier, W., Bilderbeek, U., Timmesfeld, N., von Garrel, T., Matter, H.P., 2011. Effect of storage temperature on allograft bone. Transfus. Med. Hemother. 39 (1), 36–40, http://dx.doi.org/10.1159/000335647.

Frick, C., Clark, B., Orso, S., Schneider, A., Arzt, E., 2008a. Size effect on strength and strain hardening of small-scale [111] nickel compression pillars. Mater. Sci. Eng. A 489 (August (1–2)), 319–329, http://dx.doi.org/10.1016/j.msea.2007.12.038.

Frick, C., Orso, S., Arzt, E., 2007. Loss of pseudoelasticity in nickel–titanium sub-micron compression pillars. Acta Mater. 55 (June (11)), 3845–3855, http://dx.doi.org/10.1016/j.actamat.2007.02.034.

Frick, C.P., Clark, B.G., Orso, S., Sonnweber-Ribic, P., Arzt, E., 2008b. Orientation-independent pseudoelasticity in small-scale NiTi compression pillars. Scr. Mater. 59 (July (1)), 7–10, http://dx.doi.org/10.1016/j.scriptamat.2008.01.051.

Fritsch, A., Dormieux, L., Hellmich, C., Sanahuja, J., 2009a. Mechanical behavior of hydroxyapatite biomaterials: an experimentally validated micromechanical model for elasticity and strength. J. Biomed. Mater. Res. Part A 88 (1), 149–161.

Fritsch, A., Hellmich, C., 2007. Universal microstructural patterns in cortical and trabecular, extracellular and extravascular bone materials: micromechanics-based prediction of anisotropic elasticity. J. Theor. Biol. 244 (4), 597–620.

Fritsch, A., Hellmich, C., Dormieux, L., 2009b. Ductile sliding between mineral crystals followed by rupture of collagen crosslinks: experimentally supported micromechanical explanation of bone strength. J. Theor. Biol. 260 (2), 230–252.

Gao, H., Ji, B., Jäger, I.L., Arzt, E., Fratzl, P., 2003. Materials become insensitive to flaws at nanoscale: lessons from nature. Proc. Natl. Acad. Sci. 100 (10), 5597–5600.

Gong, J.K., Arnold, J.S., Cohn, S.H., 1964. Composition of trabecular and cortical bone. Anat. Rec. 149 (3), 325–331, http://dx.doi.org/10.1002/ar.1091490303.

Hamed, E., Jasiuk, I., 2013. Multiscale damage and strength of lamellar bone modeled by cohesive finite elements. J. Mech. Behav. Biomed. Mater. 28, 94–110.

Hammett, F.S., 1925. A biochemical study of bone growth: I. Changes in the ash, organic matter, and water during growth (mus norvegicus albinus). J. Biol. Chem. 64 (2), 409–428.

Hansen, N., Schreyer, H., 1994. A thermodynamically consistent framework for theories of elastoplasticity coupled with damage. Int. J. Solids Struct. 31 (3), 359–389.

Hellmich, C., Barthélémy, J.-F., Dormieux, L., 2004a. Mineral-collagen interactions in elasticity of bone ultrastructure—a continuum micromechanics approach. Eur. J. Mech. A/Solids 23 (5), 783–810.

Hellmich, C., Ulm, F., 2005a. Microporodynamics of bones: prediction of the Frenkel–Biot slow compressional wave. J. Eng. Mech. 131 (9), 918–927, http://dx.doi.org/10.1061/(ASCE)0733-9399(2005)131:9(918).

Hellmich, C., Ulm, F.-J., 2003. Average hydroxyapatite concentration is uniform in the extracollagenous ultrastructure of mineralized tissues: evidence at the 1–10-μm scale. Biomech. Model. Mechanobiol. 2 (1), 21–36.

Hellmich, C., Ulm, F.-J., 2005b. Drained and undrained poroelastic properties of healthy and pathological bone: a poro-micromechanical investigation. Transp. Porous Media 58 (3), 243–268, http://dx.doi.org/10.1007/s11242-004-6298-y.

Hellmich, C., Ulm, F.-J., Dormieux, L., 2004b. Can the diverse elastic properties of trabecular and cortical bone be attributed to only a few tissue-independent phase properties and their interactions? Biomech. Model. Mechanobiol. 2 (4), 219–238, http://dx.doi.org/10.1007/s10237-004-0040-0.

Hengsberger, S., Kulik, A., Zysset, P., 2002. Nanoindentation discriminates the elastic properties of individual human bone lamellae under dry and physiological conditions. Bone 30 (1), 178–184.

Hoffler, C., Guo, X., Zysset, P.K., Moore, K.E., Goldstein, S.A., 1997. Evaluation of bone microstructural properties: effect of testing conditions, depth, repetition, time delay and displacement rate. In: Proceedings of the 1997 Bioengineering conference, ASME, Sunriver, vol. 35. pp. 567–568, 〈http://www.scopus.com/inward/record.url?eid=2-s2.0-0030717285&partnerID=40&md5=5d20a6804071b91b1f1aacd4400090c3〉.

Jimenez-Palomar, I., Shipov, A., Shahar, R., Barber, A.H., 2012. Influence of SEM vacuum on bone micromechanics using in situ AFM. J. Mech. Behav. Biomed. Mater. 5 (January (1)), 149–155, http://dx.doi.org/10.1016/j.jmbbm.2011.08.018.

Kachanov, L., 1986. Introduction to Continuum Damage Mechanics, vol. 10. Kluwer Academic Publishers, Dordrecht, The Netherlands.

Katsamenis, O.L., Chong, H.M., Andriotis, O.G., Thurner, P.J., 2013. Load-bearing in cortical bone microstructure: selective stiffening and heterogeneous strain distribution at the lamellar level. J. Mech. Behav. Biomed. Mater. 17, 152–165.

Kheradmand, N., Vehoff, H., Barnoush, A., 2013. An insight into the role of the grain boundary in plastic deformation by means of a bicrystalline pillar compression test and atomistic simulation. Acta Mater. 61 (November (19)), 7454–7465, http://dx.doi.org/10.1016/j.actamat.2013.08.056.

Kim, H., Rey, C., Glimcher, M., 1996. X-ray diffraction, electron microscopy, and Fourier transform infrared spectroscopy of apatite crystals isolated from chicken and bovine calcified cartilage. Calcif. Tissue Int. 59 (1), 58–63, http://dx.doi.org/10.1007/s002239900086.

Kim, H.-M., Rey, C., Glimcher, M.J., 1995. Isolation of calcium-phosphate crystals of bone by non-aqueous methods at low temperature. J. Bone Miner. Res. 10 (10), 1589–1601, http://dx.doi.org/10.1002/jbmr.5650101021.

Kinashi, H., Nagoshi, T., Chang, T.-F. M., Sato, T., Sone, M., 2014. Mechanical properties of Cu electroplated in supercritical CO_2 emulsion evaluated by micro-compression test. Microelectron. Eng. 121 (June), 83–86, http://dx.doi.org/10.1016/j.mee.2014.03.029.

Kirchlechner, C., Keckes, J., Motz, C., Grosinger, W., Kapp, M., Micha, J., Ulrich, O., Dehm, G., 2011. Impact of instrumental constraints and imperfections on the dislocation structure in micron-sized Cu compression pillars. Acta Mater. 59 (August (14)), 5618–5626, http://dx.doi.org/10.1016/j.actamat.2011.05.037.

Ko, C.-C., Douglas, W.H., Cheng, Y.-S., 1995. Intrinsic mechanical competence of cortical and trabecular bone measured by nanoindentation and microindentation probes. In: American Society of Mechanical Engineers, Bioengineering Division (Publication) BED, vol. 29, pp. 415–416, 〈www.scopus.com〉.

Lees, S., 1982. Ultrasonic measurements of deer antler, bovine tibia and tympanic bulla. J. Biomech. 15 (11), 867–874.

Lees, S., 1987. Considerations regarding the structure of the mammalian mineralized osteoid from viewpoint of the generalized packing model. Connect. Tissue Res. 16 (4), 281–303.

Lees, S., 2003. Mineralization of type I collagen. Biophys. J. 85, 204–207.

Lees, S., Ahern, J., Leonard, M., 1983. Parameters influencing the sonic velocity in compact calcified tissues of various species. J. Acoust. Soc. Am. 74, 28–33.

Lees, S., Bonar, L.C., Mook, H.A., 1984. A study of dense mineralized tissue by neutron diffraction. Int. J. Biol. Macromol. 6 (6), 321–326.

Lees, S., Hanson, D., Page, E.A., 1995. Some acoustical properties of the otic bones of a fin whale. J. Acoust. Soc. Am. 99 (4), 2421–2427.

Lees, S., Hanson, D., Page, E.A., Mook, H., 1994. Comparison of dosage-dependent effects of beta-aminopropionitrile, sodium fluoride, and hydrocortisone on selected physical properties of cortical bone. J. Bone Miner. Res. 9 (9), 1377–1389.

Lees, S., Heeley, J.D., Cleary, P.F., 1979. A study of some properties of a sample of bovine cortical bone using ultrasound. Calcif. Tissue Int. 29 (1), 107–117.

Linde, F., Sørensen, H.C.F., 1993. The effect of different storage methods on the mechanical properties of trabecular bone. J. Biomech. 26 (10), 1249–1252.

Luczynski, K.W., Brynk, T., Ostrowska, B., Swieszkowski, W., Reihsner, R., Hellmich, C., 2013. Consistent quasistatic and acoustic elasticity determination of poly-l-lactide-based rapid-prototyped tissue engineering scaffolds. J. Biomed. Mater. Res. Part A 101 (1), 138–144.

Lurie, A., Belyaev, A., 2005. Theory of Elasticity. Foundations of Engineering Mechanics. Springer, Berlin.

Mandel, J., 1966. Cours de mécanique des milieux continus. Gauthier-Villars, Paris, France 〈http://books.google.fr/books?id=xrzPAAAAMAAJ〉.

McCarthy, R., Jeffcott, L., McCartney, R., 1990. Ultrasound speed in equine cortical bone: effects of orientation, density, porosity and temperature. J. Biomech. 23 (11), 1139–1143.

Monnet, G., Pouchon, M.A., 2013. Determination of the critical resolved shear stress and the friction stress in austenitic stainless steels by compression of pillars extracted from single grains. Mater. Lett. 98 (May), 128–130, http://dx.doi.org/10.1016/j.matlet.2013.01.118.

Morin, C., Hellmich, C., 2013. Mineralization-driven bone tissue evolution follows from fluid-to-solid phase transformations in closed thermodynamic systems. J. Theor. Biol. 335, 185–197.

Morin, C., Hellmich, C., 2014. A multiscale poromicromechanical approach to wave propagation and attenuation in bone. Ultrasonics 54 (July (5)), 1251–1269, http://dx.doi.org/10.1016/j.ultras.2013.12.005.

Morin, C., Hellmich, C., Henits, P., 2013. Fibrillar structure and elasticity of hydrating collagen: a quantitative multiscale approach. J. Theor. Biol. 317, 384–393.

Mutoh, M., Nagoshi, T., Mark Chang, T.-F., Sato, T., Sone, M., 2013. Micro-compression test using non-tapered micro-pillar of electrodeposited Cu. Microelectron. Eng. 111 (November), 118–121, http://dx.doi.org/10.1016/j.mee.2013.02.040.

Nagoshi, T., Chang, T.-F.M., Tatsuo, S., Sone, M., 2013. Mechanical properties of nickel fabricated by electroplating with supercritical CO_2 emulsion evaluated by micro-compression test using non-tapered micro-sized pillar. Microelectron. Eng. 110 (October), 270–273, http://dx.doi.org/10.1016/j.mee.2013.02.001.

Nagoshi, T., Shibata, A., Todaka, Y., Sato, T., Sone, M., 2014. Mechanical behavior of a microsized pillar fabricated from ultrafine-grained ferrite evaluated by a microcompression test. Acta Mater. 73 (July), 12–18, http://dx.doi.org/10.1016/j.actamat.2014.03.048.

Nalla, R., Porter, A., Daraio, C., Minor, A., Radmilovic, V., Stach, E., Tomsia, A., Ritchie, R., 2005. Ultrastructural examination of dentin using focused ion-beam cross-sectioning and transmission electron microscopy. Micron 36 (7–8), 672–680 〈http://www.sciencedirect.com/science/article/pii/S0968432805001174〉.

Nazarian, A., Hermannsson, B., Muller, J., Zurakowski, D., Snyder, B.D., 2009. Effects of tissue preservation on murine bone mechanical properties. J. Biomech. 42 (1), 82–86.

Ng, K., Lin, Y., Ngan, A., 2011. Compression of micron-sized pillars of anodic aluminium oxide nano-honeycomb. J. Mech. Phys. Solids 59 (February (2)), 251–264, http://dx.doi.org/10.1016/j.jmps.2010.10.008.

Ng, K., Ngan, A., 2008. Stochastic nature of plasticity of aluminum micro-pillars. Acta Mater. 56 (May (8)), 1712–1720, http://dx.doi.org/10.1016/j.actamat.2007.12.016.

Nicolella, D.P., Ni, Q., Chan, K.S., 2011. Non-destructive characterization of microdamage in cortical bone using low field pulsed NMR. J. Mech. Behav. Biomed. Mater. 4 (3), 383–391.

Nobakhti, S., Limbert, G., Thurner, P.J., 2014. Cement lines and interlamellar areas in compact bone as strain amplifiers—contributors to elasticity, fracture toughness and mechanotransduction. J. Mech. Behav. Biomed. Mater. 29, 235–251.

O'Brien, F., Taylor, D., Dickson, G., Lee, T., 2000. Visualisation of three-dimensional microcracks in compact bone. J. Anat. 197 (3), 413–420 〈http://www.scopus.com/inward/record.url?eid=2-s2.0-0033645973&partnerID=40&md5=72268f0d74899a483635b3f6b366996c〉.

O'Brien, F.J., Taylor, D., Lee, T., 2003. Microcrack accumulation at different intervals during fatigue testing of compact bone. J. Biomech. 36 (7), 973–980.

Oliver, W., Pharr, G.M., 1992. An improved technique for determining hardness and elastic modulus using load and displacement sensing indentation experiments. J. Mater. Sci. 7 (6), 1564–1583.

Pichler, B., Hellmich, C.A., Mang, H., 2007. A combined fracture-micromechanics model for tensile strain-softening in brittle materials, based on propagation of interacting microcracks. Int. J. Numer. Anal. Methods Geomech. 31 (2), 111–132 http://dx.doi.org/10.1002/nag.544.

Raghavan, R., Adusumalli, R.-B., Buerki, G., Hansen, S., Zimmermann, T., Michler, J., 2012. Deformation of the compound middle lamella in spruce latewood by micro-pillar compression of double cell walls. J. Mater. Sci. 47 (August (16)), 6125–6130, http://dx.doi.org/10.1007/s10853-012-6531-y.

Reilly, D.T., Burstein, A.H., Frankel, V.H., 1974. The elastic modulus for bone. J. Biomech. 7 (3), 271–275.

Reilly, G., Currey, J., 1999. The development of microcracking and failure in bone depends on the loading mode to which it is adapted. J. Exp. Biol. 202 (5), 543–552.

Rho, J.-Y., Pharr, G.M., 1999. Effects of drying on the mechanical properties of bovine femur measured by nanoindentation. J. Mater. Sci.: Mater. Med. 10 (8), 485–488.

Rho, J.-Y., Roy, M.E., Tsui, T.Y., Pharr, G.M., 1999a. Elastic properties of microstructural components of human bone tissue as measured by nanoindentation. J. Biomed. Mater. Res. 45 (1), 48–54.

Rho, J.-Y., Tsui, T.Y., Pharr, G.M., 1997. Elastic properties of human cortical and trabecular lamellar bone measured by nanoindentation. Biomaterials 18 (20), 1325–1330.

Rho, J.Y., Zioupos, P., Currey, J.D., Pharr, G.M., 1999b. Variations in the individual thick lamellar properties within osteons by nanoindentation. Bone 25 (3), 295–300.

Ritchie, R., 2011. The conflicts between strength and toughness. Nat. Mater. (10), 817–822.

Roy, M., Rho, J.-Y., Tsui, T., Pharr, G., 1996. Variation of Young's modulus and hardness in human lumbar vertebrae measured by nanoindentation. In: Proceedings of the Bioengineering conference, ASME BED, vol. 33. pp. 385–386, 〈http://www.scopus.com/inward/record.url?eid=2-s2.0-0030387534&partnerID=40&md5=6d6457f84729eec4bea305bbd416ec1b〉.

Salençon, J., 2001. Handbook of Continuum Mechanics: General Concepts-thermoelasticity. Springer, Berlin, Heidelberg, New York.

Sasso, M., Haiat, G., Yamato, Y., Naili, S., Matsukawa, M., 2008. Dependence of ultrasonic attenuation on bone mass and microstructure in bovine cortical bone. J. Biomech. 41, 347–355.

Schaffler, M., Choi, K., Milgrom, C., 1995. Aging and matrix microdamage accumulation in human compact bone. Bone 17 (6), 521–525.

Schaffler, M., Pitchford, W., Choi, K., Riddle, J., 1994. Examination of compact bone microdamage using back-scattered electron microscopy. Bone 15 (5), 483–488.

Schneider, A., Clark, B., Frick, C., Gruber, P., Arzt, E., 2009. Effect of orientation and loading rate on compression behavior of small-scale Mo pillars. Mater. Sci. Eng. A 508 (May (1–2)), 241–246, http://dx.doi.org/10.1016/j.msea.2009.01.011.

Schneider, A., Frick, C., Clark, B., Gruber, P., Arzt, E., 2011. Influence of orientation on the size effect in bcc pillars with different critical temperatures. Mater. Sci. Eng. A 528 (January (3)), 1540–1547, http://dx.doi.org/10.1016/j.msea.2010.10.073.

Schneider, A., Kiener, D., Yakacki, C., Maier, H., Gruber, P., Tamura, N., Kunz, M., Minor, A., Frick, C., 2013. Influence of bulk pre-straining on the size effect in nickel compression pillars. Mater. Sci. Eng. A 559 (January), 147–158, http://dx.doi.org/10.1016/j.msea.2012.08.055.

Schwiedrzik, J., Raghavan, R., Bürki, A., LeNader, V., Wolfram, U., Michler, J., Zysset, P., 2014. In situ micropillar compression reveals superior strength and ductility but an absence of

damage in lamellar bone. Nat. Mater. 13 (June (7)), 740–747, http://dx.doi.org/10.1038/nmat3959.

Stewart, J., Jiang, L., Williams, J., Chawla, N., 2012. Prediction of bulk tensile behavior of dual phase stainless steels using constituent behavior from micropillar compression experiments. Mater. Sci. Eng. A 534 (February), 220–227, http://dx.doi.org/10.1016/j.msea.2011.11.062.

Stokes, D.J., Morrissey, F., Lich, B.H., 2006. A new approach to studying biological and soft materials using focused ion beam scanning electron microscopy (FIB SEM). J. Phys.: Conf. Ser. 26 (1), 50.

Su, X., Sun, K., Cui, F., Landis, W., 2003. Organization of apatite crystals in human woven bone. Bone 32 (2), 150–162.

Tai, K., Ulm, F-J, Ortiz, C., 2006. Nanogranular origins of the strength of bone. Nano Letters 6 (11), 2520–2525.

Turner, C.H., Rho, J., Takano, Y., Tsui, T.Y., Pharr, G.M., 1999. The elastic properties of trabecular and cortical bone tissues are similar: results from two microscopic measurement techniques. J. Biomech. 32 (4), 437–441.

Vuong, J., Hellmich, C., 2011. Bone fibrillogenesis and mineralization: quantitative analysis and implications for tissue elasticity. J. Theor. Biol. 287, 115–130.

Wenzel, T., Schaffler, M., Fyhrie, D., 1996. In vivo trabecular microcracks in human vertebral bone. Bone 19 (2), 89–95.

Yang, Y., Ye, J., Lu, J., Liu, F., Liaw, P., 2009. Effects of specimen geometry and base material on the mechanical behavior of focused-ion-beam-fabricated metallic-glass micropillars. Acta Mater. 57 (March (5)), 1613–1623, http://dx.doi.org/10.1016/j.actamat.2008.11.043.

Zaoui, A., 2002. Continuum micromechanics: survey. J. Eng. Mech. 128 (8), 808–816, http://dx.doi.org/10.1061/(ASCE)0733-9399(2002)128:8(808).

Zhang, X., Zhao, Q., Wang, S., Trejo, R., Lara-Curzio, E., Du, G., 2010. Characterizing strength and fracture of wood cell wall through uniaxial micro-compression test. Composites Part A: Appl. Sci. Manuf. 41 (May (5)), 632–638, http://dx.doi.org/10.1016/j.compositesa.2010.01.010.

Ziv, V., Weiner, S., 1994. Bone crystal sizes: a comparison of transmission electron microscopic and X-ray diffraction line width broadening techniques. Connect. Tissue Res. 30 (3), 165–175.

Zylberberg, L., Traub, W., de Buffrenil, V., Allizard, F., Arad, T., Weiner, S., 1998. Rostrum of a toothed whale: ultrastructural study of a very dense bone. Bone 23, 241–247.

Zysset, P.K., Edward Guo, X., Edward Hoffler, C., Moore, K.E., Goldstein, S.A., 1999. Elastic modulus and hardness of cortical and trabecular bone lamellae measured by nanoindentation in the human femur. J. Biomech. 32 (10), 1005–1012.